ST3Gal1 synthesis of Siglec ligands mediates anti-tumour immunity in prostate cancer

Rebecca Garnham[1], Daniel Geh[1], Ryan Nelson[2], Erik Ramon-Gill[1], Laura Wilson[2], Edward N Schmidt[4,5], Laura Walker[2], Beth Adamson[2], Adriana Buskin[2], Anastasia Hepburn[2], Kirsty Hodgson[1], Hannah Kendall[2], Fiona M Frame[3], Norman Maitland[3], Kelly Coffey[1], Craig N Robson[2], David J Elliott[1], Rakesh Heer[2], Matthew Macauley[4,5], Jennifer Munkley[1], Luke Gaughan[2], Jack Leslie[1], Emma Scott[1]*

*Correspondence to Emma Scott at emma.scott@newcastle.ac.uk

1. Newcastle University, Centre for Cancer, Newcastle University Biosciences Institute, Newcastle, NE1 3BZ, UK
2. Newcastle University, Centre for Cancer, Newcastle University Translational and Clinical Research Institute, Newcastle, NE1 3BZ, UK
3. Cancer Research Unit, Department of Biology, University of York, Heslington, North Yorkshire YO10 5DD, UK
4. Department of Chemistry, University of Alberta. Edmonton, AB, T6G 2G2, Canada
5. Department of Medical Microbiology and Immunology, University of Alberta. Edmonton, AB, T6G 2E1, Canada

Abstract

Immune checkpoint blockade trials have yet to produce a robust anti-cancer response in prostate cancer patients as a monotherapy due to the immunosuppressed prostate cancer tumour immune microenvironment. ST3Gal1 and other sialyltransferases are implicated in cancer and immune suppression by synthesizing sialoglycans, which act as ligands for Siglec receptors. These checkpoints are important for the immune response. However, it's unclear how the synthesis of Siglec ligands is regulated, and little is known about the role of sialoglycan-Siglec-axis in prostate cancer's evasion of anti-tumour immunity. We report that ST3Gal1 levels negatively correlate with androgen signalling in prostate tumours. Utilising syngeneic mouse models, we demonstrate that ST3Gal1 plays an important role in modulating tumour immune evasion. Using mouse models, patient samples and *in vitro* models we show that ST3Gal1 synthesises sialoglycans with the capacity to engage the Siglec-7 and Siglec-9 immunoreceptors preventing immune clearance of cancer cells. For the first time we provide evidence of the expression of Siglec-7/9 ligands and their respective immunoreceptors in prostate tumours. Importantly, we show that these interactions can be modulated by enzalutamide and may maintain immune suppression in enzalutamide treated tumours. We conclude that the activity of ST3Gal1 is critical to prostate cancer anti-tumour immunity and provide rationale for the use of glyco-immune checkpoint targeting therapies in advanced prostate cancer.

Introduction

Prostate cancer (PC) is the second most common male cancer worldwide, with 1.4 million men diagnosed globally in 2020 (1). During tumorigenesis, prostate tumour growth is driven by androgen receptor (AR) signalling and as such initial therapeutic options for advanced PC are hormone-based therapies which target AR signalling, such as anti-androgens (2,3). Most tumours will eventually become resistant to anti-androgen therapies and progress to castrate resistant prostate cancer (CRPC) (4). Patients who develop CRPC currently have no curative therapeutic options available to them, and with 375,000 men dying from the disease in 2020 there is a critical need to develop novel therapies for men with advanced PC (1)

An area of innovation in the search for new therapies for CRPC has been immunotherapy. In 2017, Pembrolizumab, an anti-PD-1 agent, was approved for use in solid tumours with high microsatellite instability (5). Despite this breakthrough, immune checkpoint blockade (ICB) trials have yet to elicit a robust anti-cancer response in PC patients as a monotherapy (6). There is now a focus on developing new combination therapies, capable of sensitising prostate tumours to ICB, with over 40 clinical trials investigating combination ICB therapies for PC (7–10). Enzalutamide, a commonly used second generation AR antagonist can remodel the tumour immune microenvironment (TIME) (11). Combination enzalutamide-immunotherapies are now in clinical trial for CRPC (12,13). Results from early phase trials demonstrated a durable therapeutic response in only 18% of participants (12,13). Clearly, there are underlying mechanisms which prevent cancers responding to current combination therapies. For ICB to be successful in PC, novel treatments need to be developed to target the vast majority of non-responders.

Recently, glyco-immune checkpoints have been identified as drivers of immune suppression in solid tumours and have demonstrated exciting pre-clinical potential as novel targets for combination immunotherapy strategies (14–19). Siglec receptors are broadly expressed by the immune system and engage with sialic acid to drive immune suppression (20). Although promising, response to Siglec targeting is dependent upon the local TIME, with immunosuppressive tumours, such as prostate tumours, less sensitive to Siglec targeting (21) We have previously identified AR dependant glycosylation changes in PC and have demonstrated that changes in sialyation are a feature of prostate tumours (22–25). However, the sialome (all of the sialoglycans in a cell) is highly complex and demonstrates great inter- and intra- patient heterogeneity.

Here, we determine that expression of the sialyltransferase ST3Gal1 is inversely correlated with AR signalling in prostate tumours. This led us to investigate the effect of anti-androgen therapies, namely enzalutamide on ST3Gal1 and its associated α2-3-linked sialylation patterns. Our results show that in cell models, patient samples and syngeneic mouse models, enzalutamide increases levels of ST3Gal1-driven patterns of α2-3-sialylation. We confirm that ST3Gal1 synthesises immunosuppressive Siglec-7 and Siglec-9 ligands in PC, and that their levels can be modulated by androgen deprivation therapies. We identified Siglec-7/9 on immunosuppressive macrophages in prostate tumours and demonstrate that removing their ligands from tumours enhances anti-tumour immunity in a mouse model. We propose that enzalutamide treatment may inadvertently upregulate these suppressive glyco-immune checkpoints and that Siglec targeting therapies may sensitise PC patients to enzalutamide-ICB combination therapies.

Materials and Methods

Human tissue sample ethics

Patient samples were collected with ethical permission from Castle Hill Hospital (Cottingham, Hull) (Ethics Number: 07/H1304/121). Use of patient tissue was approved by the Local Research Ethics Committees. Patients gave informed consent, and all patient samples were anonymized.

Bioinformatic analysis of publicly available data

Publicly available transcriptomic datasets were accessed using cBioPortal (26) or camcAPP (27). Gene set enrichment was performed using GSEA software with available data downloaded from the TCGA PRAD cohort using cBioPortal.

Cell culture and genetic modification of cell lines

Cell culture and cell lines used were as described previously (24). The stable cell lines used in the study were created by lentiviral transduction using a multiplicity of infection of 5. For details of the lentiviral particles used see Supplemental Table 3. TRAMP-C2 cells were maintained in Dulbecco's modified Eagle's medium with 4 mM L-glutamine adjusted to contain 1.5 g/L sodium bicarbonate and 4.5 g/L glucose supplemented with 0.005 mg/ml bovine insulin and 10 nM dehydroisoandrosterone, 90%; fetal bovine serum (FBS), 5%, Nu-Serum IV, 5%. For steroid deplete conditions cells were seeded in RPMI medium with L-glutamine +10% charcoal stripped FBS + 1% Pen/Strep. Cells were treated with 10 μM Enzalutamide (Selleckchem) or 10 nM R1881 for 24 hours.

Colony formation assay

$1x10^3$ cells were plated into a single well of a 6 well dish. Colonies were allowed to grow for 3 weeks with the medium replaced at regular intervals. Colonies were fixed with 100% methanol and stained with crystal violet (0.05% w/v). Colony numbers were counted by eye and recorded.

WST-1 assay

$5x10^3$ cells were plated in to a single well of a 96 well culture plate. At 24, 48 or 72 hours WST-1 reagent (Cambridge Bio) was added to each well and incubated at 37°C for 2 hours. Cell viability was detected at 450 nm wavelength using a Thermofisher Scientific Variskan LUX microplate reader.

Spheroid experiments

Single cell suspension was seeded onto the underside of a 15cm culture dish lid, in full growth media, at a density of $3x10^3$ cells per 20µl. The lid was inverted and placed onto the dish which contained 10ml PBS. Cells were allowed to form spheroids for four days. Spheroid formation and size was measured using a LeciaDM6 microscope.

Detection of ST3Gal1 by ELISA

Human ST3Gal1 sandwich pre-validated ELISA kits were purchased from Cambridge Bioscience (RayBioTech, ELH-ST3GAL1). Samples and standards were assayed in duplicate according to the manufacturer's protocol.

Mouse models

All experiments were performed in accordance with a UK Home Office licence (PC02CF4AB), adhered to ARRIVE guidelines and in accordance with the UK Animal (Scientific Procedures) Act 1986. Experiments were subject to review by the animal welfare and ethical review board of Newcastle University. All mice were housed with unrestricted access to food and water and maintained on a constant 12hours light-dark cycle.

Male C57BL/6 mice (7 weeks old) were purchased from either Envigo or Charles River (UK). For TRAMP-C2 NT and *St3gal1*$^{-/-}$ subcutaneous xenografts, 8-week-old mice were injected subcutaneously with $2x10^6$ cells in the right flank. For TRAMP-C2 enzalutamide studies, 2 x 10^6 TRAMP-C2 cells were engrafted by subcutaneous injection into the right flank of C57BL/6 mice and allowed to establish tumours. Once tumours were established, animals were randomly allocated to vehicle or treatment groups and received a dose of 20 mg/kg

enzalutamide or a DMSO vehicle control by oral gavage once daily, at the indicated time point. For immune depletion studies tumour measurements and body weights were taken three times a week. Tumour volume measurements were determined using the formula $l \times w \times h$.

For immune depletion studies mice were randomly allocated to IgG control, anti-CSFR1 or anti-CD8α groups. C57BL/6 mice received 200 µg IgG control, anti-CSFR or anti-CD8 twice weekly by intraperitoneal injection, starting at the indicated time point. 5×10^6 TRAMP-C2 *St3gal1*$^{-/-}$ cells were injected into the right flank of mice subcutaneously 7 days after depletion began.

Flow cytometry on tumours and blood

Blood samples were collected into EDTA coated tubes (BD Biosciences) and treated with lysing buffer (BD Biosciences). Tumours were collected into cold PBS then manually cut into small pieces and digested in GentleMACS C dissociation tubes using the GentleMACS tissue dissociator (Miltenyi Biotec) with the manufacture's enzymes (liver dissociation kit, Miltenyi Biotec). Following generation of single cell suspension enzymes were neutralised with cold RMPI and passed through a 100µm cell strainer. Debris/ dead cells were removed using a 30% percoll gradient and centrifugation. Tumour single cell suspensions were then treated with RBC lysis buffer (BD Biosciences). Single cell suspensions were stained with cell viability dye (Invitrogen, LIVE/DEAD fixable blue dead cell stain kit) then blocked with anti-CD16/32 purified antibody at 1:100 for 10 mins (Biolegend). Samples were stained with directly conjugated antibodies (see below) for 30 minutes at 4°C then fixed in 4% paraformaldehyde. All samples were run on the BD FACSymphony flow cytometer using BD FACSDiva™ software. Data was analysed with FlowJo 10.7.1 software. For high dimensional analysis 10,000 random cells from the CD45$^+$Live leukocyte gate from each sample were down-sampled and concatenated. tSNE maps were generated using the tSNE add on, encompassing all parameters excluding FSC, SSC, Dead and CD45.

All antibodies were purchased from Biolegend apart from; CD11b-BV510, SIRPα-BV711, NK1.1-BV750, Ly6G-BUV395, F4/80-BUV661, CD86-BUV563, CD19-BUV805, SiglecE-BUV615 which were purchased from BD Biosciences. Siglec-E panel: CD4-FITC (1:100, RM4-5), Ly6C-PerCP-Cy5.5 (1:800, HK1.4), PD1-PE (1:100, 29F.1A12), CXCR2-PE/Dazzle 594 (1:100, SA045E1), CD103-Pe-Cy5 (1:100, 2E7), CD3-PE-Cy7 (1:100, 17A2), IA/IE-APC (1:100, M5/114.15.2), SiglecG-R718 (1:100, SH1), CD8α-APC-Cy7 (1:100, 53-6.7), CD197-BV421 (1:100, 4B12), CD11b-BV510 (1:100, M1/70), CD45-BV570 (1:100, 30-F11), CD11c-BV605 (1:100, N418), PDL1-BV650 (1:100, 10F.962), SIRPα-BV711 (1:100, P84), NK1.1-BV711 (1:100, PK136), XCR1-BV785 (1:100, ZET), Ly6G-BUV395 (1:100, 1A8), CD86-

BUV563 (1:100, PO3), SiglecE-BUV615 (1:100, 750620), F4/80-BUV661 (T45-2342), CD19-BUV805 (1:100, 1D3). CD8 and CSFR1 depletion confirmation panel: CD4-FITC (1:100, RM4-5), Ly6C-PerCP-Cy5.5 (1:800, HK1.4), CD3-PE-Cy7 (1:100, 17A2), CD45-AF700 (1:100, 30-F11), CD8α-APC-Cy7 (1:100, 53-6.7), CD11b-BV510 (1:100, M1/70), CD115-BV711 (1:100, AFS98), Ly6G-BUV395 (1:100, 1A8), F4/80-BUV661 (T45-2342), CD19-BUV805 (1:100, 1D3).

Lectin flow cytometry

MAL-II expression was analysed using the MAL-II lectin (Vector Laboratories, B-1305-2) conjugated to streptavidin AlexaFluor 647 (Abcam). $1x10^5$ cells were pelleted by centrifugation, washed in PBS-T, resuspended in 1X carbo-free blocking solution (Vector Laboratories) and labelled with 2 µg/mL MAL-II lectin for 30 minutes at 4°C. Cells were washed and stained with streptavidin Alexa Fluor 647 (Abcam) for 15 minutes at 4°C, before repeating washes and resuspending in PBS. Propidium iodine was used to discriminate between live and dead cells and cells were processed through a FACSymphony flow cytometer.

Siglec-Fc flow cytometry

$1x10^5$ cells were pelleted by centrifugation, washed in cold PBS-T, resuspended in 1X carbo-free blocking solution (Vector Laboratories) and labelled with Siglec-Fcs purchased from R&D or reagents described previously (28). Provided reagents were pre-complexed to Strep-tactin-AF647 in the dark for 30 minutes at 4°C. Purchased Siglec-Fcs were incubated with cells for 30 minutes at 4°C, washed 3 times and then stained with an anti-human Alexa Fluor 647 secondary antibody for 15 minutes. Cells were washed 3 times in PBS, incubated with propidium iodine to discriminate between live and dead cells and processed through a FACSymphony flow cytometer.

Immunocytochemistry

Cells were washed and fixed using 100% methanol at 4°C. Next, slides were washed in PBS and blocked with 10% goat serum for 1 hour at RT with gentle rocking. After brief washing with PBS-T, cells were incubated with anti-ST3GAL1 (Invitrogen, PA5-21721, 1:200) antibody diluted in 10% goat serum block overnight. Slides were washed extensively with PBS-T and incubated with an Alexa Fluor 594-goat anti-mouse secondary antibody (Invitrogen). Finally, washes were repeated before counterstaining with Hoechst 33342 (Thermo Fisher Scientific). Images were obtained with fixed exposure times using a ZEISS AxioImager 2 microscope.

Immunohistochemistry

Heat mediated antigen retrieval was performed in 10 mM citrate pH 6.0 followed by staining with the appropriate antibody. Antibody dilutions are shown in Supplementary Table 1. Sections were counterstained with haematoxylin. H-Scores were calculated using the Aperio Slide Scanner scoring intensity for only epithelial cells with positive staining.

Immunofluorescence on FFPE tissue

After dewaxing and rehydration in graded alcohol, human prostate cancer FFPE slides were washed with PBS and heated at 121°C for 15 minutes in Tris-EDTA for epitope retrieval. Slides were blocked in 10% goat serum for 1 hour at RT and incubated overnight with the primary antibodies in blocking solution at 4°C. The following primary antibodies were used: anti-Siglec-9 (Proteintech,13377-1-AP, 1:200) anti-Siglec-7 (Proteintech, 13939-1-AP, 1:200), anti-CD14 (Proteintech, 60253-1-Ig, 1:500), anti-CD163 (Invitrogen, MA511458, 1:500) anti-AMACR (Proteintech,15918-1-AP, 1:500) overnight at 4°C. After washing in PBS-T, samples were incubated with goat anti-rabbit Alexa Fluor 647 or donkey anti-mouse Alexa Fluor 488 (Invitrogen) for 60 minutes at room temperature. Images were obtained using a ZEISS AxioImager 2 microscope.

Western blotting

Western blotting was performed as previously described (29). For details of the antibodies used please see supplemental table 1.

Quantitative PCR

Quantitative PCR (qPCR) was performed as previously describe (24). For details of the primers used please see supplemental table 2.

Statistical Analyses

Statistical analyses were performed using GraphPad Prism 8 (GraphPad Software, Inc., San Diego, CA, USA). Statistical significance is shown as * $p < 0.05$, ** $p < 0.01$, *** $p < 0.001$ and **** $p < 0.0001$.

Results

ST3Gal1 expression inversely correlates with androgen signalling in prostate tumours

Sialylation of core-1 *O*-glycans has previously been highlighted as a feature of CRPC (30). This complex process is regulated by a range of glycosyltransferases, including ST3Gal1. We sought to investigate the expression of ST3Gal1 in PC and found protein levels to be significantly increased in prostate tumour tissue compared with healthy normal prostatic tissue

(**Figure 1A**). To understand which pathways are altered in prostate tumours with high *ST3GAL1* expression, we performed gene set enrichment (GSEA) on the cancer genome atlas (TCGA) prostate adenocarcinoma (PRAD) cohort (31). GSEA in 250 patients stratified based on *ST3GAL1* gene expression levels revealed 11 gene sets negatively enriched in *ST3GAL1*^{high} tumours (**Figure 1B**). We noted that the HALLMARK ANDROGEN RESPONSE gene set was negatively enriched in tumours with high expression of *ST3GAL1* (**Figure 1C and Supplemental Table 2**).

Given that *ST3GAL1* expression is high in tumours which have low levels of androgen signalling we sought to validate this finding using *in vitro* models. In the androgen responsive LNCaP cell line treated with R1881 (an AR ligand) protein levels of ST3Gal1 exhibited a significant decrease compared with steroid depleted controls (**Figure 1D**). In contrast, siRNA knockdown of *AR* resulted in a 3-fold increase in *ST3GAL1* levels (**Supplemental Figure 1A**). Several different clinically relevant *AR* isoforms, commonly termed AR variants, have been identified (32–36). We next looked at the effect of AR variants on expression of *ST3GAL1*. Selective knockdown of AR variants resulted in a significant increase in *ST3GAL1* mRNA levels, but to a lesser extent than knockdown of the full-length *AR* (**Figure 1E**). In transcriptomic data from 138 CRPC tumours, levels of *ST3GAL1* gene expression were negatively correlated with *AR, KLK3, NKX3.1* and *TMPRSS2* which are markers of AR signalling activity (**Figure 1F**). (37). This finding was further validated in two independent cohorts in 492 hormone dependent tumours (**Supplemental Figure 1B**) and 208 CRPC tumours (**Supplemental Figure 1C**) (38). AR variants have been linked with the onset of CRPC, and thus we profiled the expression of *ST3GAL1* in CRPC patients. We looked in a publicly available transcriptomic dataset from 59 localised PCs and 35 CRPC patients and found *ST3GAL1* to be significantly higher in CRPC samples (**Figure G**) (39). We profiled *ST3GAL1* genomic alterations across four PC cohorts (N=2016) and found *ST3GAL1* is amplified in ~8% of patients in two hormone dependant PC cohorts and amplified in ~20% of patients in two CRPC cohorts (**Figure 1H**) (38). When we stratified 500 patients based on *ST3GAL1* genomic alterations, we found that patients with an *ST3GAL1* amplification have a significantly poorer disease-free survival (p=0.007) (**Figure 1I**). Taken together, we show that *ST3GAL1* is inversely correlated with AR signalling in prostate tumours and is upregulated in CRPC.

Androgen receptor antagonism increases ST3Gal1 and α2-3-linked sialoglycans

To further examine the concept that ST3Gal1 is negatively correlated with AR signalling and subsequently increased in CRPC, we asked whether therapeutic targeting of the AR would

increase levels of ST3Gal1. LNCaP cells treated with enzalutamide had significantly elevated levels of ST3Gal1, with both mRNA and protein levels increased more than 2-fold (**Figure 2A-B**). ST3Gal1 is responsible for the terminal sialylation of core 1 and core 2 *O*-GalNAc glycans (40). It catalyses the addition of sialic acid from the nucleotide sugar donor CMP to galactose residues on target glycoproteins through an α2-3-linkage (41). We quantified cell surface levels of α2-3-linked sialic acid using the Maackia Amurensis Lectin II (MAL-II) lectin, which showed a decrease in α2-3-sialyation in cells treated with neuraminidase (an enzyme which removes sialic acid) (**Supplemental Figure 2A**). We observed a significant increase in α2-3 sialylation on the surface of LNCaP cells treated with enzalutamide (**Figure 2C**) (42,43).

We next validated our findings in a syngeneic allograft mouse model of PC. The androgen sensitive TRAMP-C2 cell line was implanted subcutaneously in C57BL/6 mice and when tumours were established mice were treated daily with 20 mg/kg enzalutamide for 1 week (**Figure 2D**). Enzalutamide treatment resulted in a decrease in tumour growth rate (**Figure 2E**) and when excised, tumours were 38% smaller than vehicle treated controls (**Figure 2F**). *St3gal1* mRNA levels in enzalutamide treated TRAMP-C2 allografts were significantly upregulated compared with vehicle treated tumours (**Figure 2G**). Enzalutamide treatment of TRAMP-C2 cells increased α2-3-sialylation of *O*-glycans both *in vitro* (**Figure 2H**) and *in vivo* (**Figure 2I**). Immune phenotyping of vehicle and enzalutamide treated allografts by high-parameter flow cytometry showed re-education of the TIME and we noted a significant 2.14-fold increase in $CD8^+$ T cells (**Figure 2J and Supplemental Figure 2B**). Transcriptomic data on matched patient biopsies treated with enzalutamide showed that *ST3GAL1* mRNA levels were significantly increased post treatment (**Figure 2K**) (11). In the same study, matched paracancerous tissue from patients pre- and post-enzalutamide treatment showed no significant increase in *ST3GAL1* levels following treatment (**Supplemental Figure 2C**), suggesting that the observed increase in *ST3GAL1* is specific to prostate tumours. These findings together demonstrate that antiandrogens such as enzalutamide can increase expression of ST3Gal1 and α2-3-sialylation of *O*-glycans both *in vitro* and *in vivo*.

St3gal1-null TRAMP-C2 cells fail to grow C57BL/6 mice

We next determined the effects of St3gal1 on tumour growth in a syngeneic allograft model of PC. We used sgRNAs targeting murine *St3gal1* to generate *St3gal1*$^{-/-}$ TRAMP-C2 cells. We confirmed successful gene knockout of *St3gal1* in TRAMP-C2 and a subsequent reduction in α2-3-sialylation (**Supplemental Figure 3A-B**). Loss of St3gal1 in TRAMP-C2-C57BL/6 allografts resulted in a 0% engraftment rate, compared with 100% engraftment of non-targeting sgRNA (NT) control cells. When mice containing *St3gal1*$^{-/-}$ TRAMP-C2 cells were

culled and harvested at day 47 there were no signs of early tumour formation (**Figure 3A-B**). NT cells grew as expected (**Figure 1C**).

We observed no significant difference in cellular proliferation or colony forming ability between *St3gal1*$^{-/-}$ and NT cells *in vitro* (**Supplemental Figure 3C-D**). Given the role of sialoglycans, and St3gal1 more specifically, in adhesion and integrin biology we assessed whether *St3gal1*$^{-/-}$ cells could form three-dimensional (3D) structures *in vitro* in the form of spheroids (44–46). *St3gal1*$^{-/-}$ cells did form spheroids and we observed a slight increase in the numbers of spheroids formed compared with NT controls (**Figure 3D**).

We confirmed our findings in human cell models. We generated stable ST3Gal1 overexpression lines in both CWR22Rv1 and LNCaP cells (LNCaP data shown in **Supplemental Figure 3G-J**). We confirmed a significant increase in *ST3GAL1* mRNA (**Supplemental Figure 3E**) and ST3Gal1 protein levels (**Figure 3E and Supplemental Figure 3F**). We next demonstrated that ST3Gal1 overexpression resulted in an increase in cell surface α2-3-sialoglycans (**Figure 3F**). ST3Gal1 overexpression did not alter cell proliferation or colony forming efficiency in either CWR22Rv1 (**Figure 3G-H**) or LNCaP cells (**Supplemental Figure 3K-L**). To confirm our findings, we generated stable *ST3GAL1* knockdown cells using lentivirus in LNCaP and CWR22Rv1 cells (CWR22Rv1 data shown in **Supplemental Figure 3N-O**). We confirmed successful knockdown of *ST3GAL1* at the gene level (**Supplemental Figure 3M**), and protein level (**Figure 3I**) and a significant reduction in cell surface α2-3-sialylyation (**Figure 3J**). In support of our previous findings, gene knockdown of *ST3GAL1* did not affect cellular proliferation or colony forming ability in LNCaP cells (**Figure 3K-L**) or CWR22Rv1 cells (**Supplemental Figure 3P-Q**). Our findings demonstrate that although we found that ST3Gal1 levels did not affect proliferative capacity *in vitro*, St3gal1-null cells fail to grow in immunocompetent mice.

Siglec-7 and Siglec-9 ligands are synthesised by ST3Gal1 and upregulated by AR targeting therapies

Given our conflicting *in vivo* and *in vitro* cell behaviour studies alongside previous studies suggesting that ST3Gal1-associated sialylation promotes tumour immune evasion in breast cancer, we hypothesised that *St3gal1*-null cells failed to engraft in immunocompetent mice as a result of immune clearance (47). Sialic acid found on tumour cell can act as a ligand for immunosuppressive Siglec receptors (17,20,48–52). Sialic acid containing glycans capable of engaging Siglec receptors can be probed using Siglec-Fc reagents. We used a panel of commercially available and specifically engineered Siglec-Fcs to profile Siglec ligands in

empty vector (EV) and sh*ST3GAL1* knockdown LNCaPs (**Figure 4A and Supplemental Figure 4A**) (28). For engineered Siglec-Fcs, mutated Siglec-Fcs, that are incapable of binding sialic acid, were used as negative controls (example shown in **Supplemental Figure 4B**) (28). We detected a significant reduction in Siglec-7 and -9 ligands in cells with loss of ST3Gal1. This was independently confirmed in CWR22Rv1 cells (**Figure 4B-C**). We also show that overexpression of ST3Gal1 in CWR22Rv1 cells increased surface expression of Siglec-7/9 ligands (**Supplemental Figure 4C**). This is in agreement with previous data generated in pancreatic ductal adenocarcinoma cells (18).

Given that ST3Gal1 modulates levels of cell surface Siglec-7 and Siglec-9 ligands in PC cells, we asked whether these ligands are expressed in PC patient biopsies. In prostate tumours, we found that both Siglec-7 and Siglec-9 ligands co-localised with α-methylacyl-CoA racemase (AMACR), suggesting that they are found in cancerous glands within the prostate (**Figure 4D-E**). As our previous data revealed that ST3Gal1 is upregulated by enzalutamide, we hypothesised that anti-androgen therapies would increase levels of Siglec-7/9 ligands. Indeed, surface Siglec-7 and -9 ligand levels increased in LNCaP cells following enzalutamide treatment (**Figure 4F-G**). We examined expression of Siglec-9 ligands in fifty patients who were treatment naïve or had received androgen deprivation therapy (ADT). Patients exposed to ADT had a significant 95% increase in expression of immunosuppressive Siglec-9 ligands (**Figure 4H**). We next quantified numbers of Siglec-9$^+$ cells in treatment naïve patients and those who had received hormone therapies and found significantly more Siglec-9$^+$ cells in treated patients (**Figure 4I**). Here we show that ST3Gal1 synthesises key glyco-immune checkpoints in PC which are upregulated following standard of care hormone therapies.

ST3Gal1-biosynthesised Siglec ligands are critical glyco-immune checkpoints in prostate cancer

To date, little is known about the expression of Siglec receptors in PC. Siglec-7 and -9 have previously been shown to be expressed on myeloid cells, including macrophages, neutrophils and NK cells (53–58). Macrophages are the most abundant immune cell type found in prostate tumours and CD163$^+$ macrophages are predictive of a poorer prognosis (59). Single-cell profiling of prostate tumour associated macrophages identified 3 distinct populations: pro-inflammatory, anti-inflammatory, and pro-proliferative macrophages with the latter two populations being predictive of a poorer prognosis (60). In an independent cohort of 208 CRPC patients, we found a strong positive correlation between *SIGLEC7* and *SIGLEC9*, and both markers positively correlated with markers of poorly prognostic macrophages (**Figure 5A**). Our analysis identified two clusters of genes which align to the pro-proliferative (highlighted in

black box) and anti-inflammatory (highlighted in red box) macrophage populations and found that both *SIGLEC7* and *SIGLEC9* cluster with an anti-inflammatory macrophage gene signature. We confirmed that Siglec-9 is co-expressed with $CD14^+$ (a myeloid marker) (**Figure 5B**) and $CD163^+$ (alternatively activated macrophage marker) (**Figure 5C**) in PC patient biopsies.

Transcriptomic analysis of PC patients using camcAPP (27) revealed that mRNA levels of both *SIGLEC7* and *SIGLEC9* are significantly elevated in Gleason grade 9 (4+5) prostate tumours when compared with lower grade tumours (**Figure 5D-E**). When we stratified 500 PC patients based on *SIGLEC7* and *SIGLEC9* gene expression, patients with high expression of *SIGLEC7* or *SIGLEC9* had a significantly reduced disease-free survival (**Figure 5F-G**). These findings were validated in a second cohort where increased *SIGLEC7* or *SIGLEC9* expression is associated with a reduction in time to biochemical reoccurrence (**Supplemental Figure 5A-B**). Thus, Siglec-7 and -9 are expressed by immunosuppressive macrophages in PC and may contribute to a significantly poorer disease prognosis.

Siglec-E is considered a Siglec-7 and Siglec-9 ortholog/paralog in mice (61). Siglec-E has been broadly described as a key glyco-immune checkpoint in multiple cancers and targeting of Siglec-E has been shown to repolarise immunosuppressive macrophages towards pro-inflammatory phenotype (15,61,62). We profiled expression of Siglec-E throughout the TIME in our syngeneic allograft model. We found Siglec-E to be highly expressed by myeloid cells (**Figure 5H**). We observed low Siglec-E expression on classic anti-tumour effector cells such $CD8^+$ T cells and NK cells in both the blood and tumour (**Figure 5I**). In contrast, we observed high levels of Siglec-E found on intratumoural macrophages. In support of our human data, Ly6C- macrophages, classically thought to be suppressive, exhibited higher Siglec-E expression than $Ly6C^+$ pro-inflammatory subsets.

We next set out to test the hypothesis that ST3Gal1 and its associated sialoglycan patterns interact with the immune system to dampen anti-tumour immunity by selectively depleting key components of the immune system. As the major effector cells of anti-tumour immunity, we targeted $CD8^+$ T cells. We also targeted macrophages given their high expression of the glyco-immune checkpoint Siglec-E. $CD8^+$ T cells and depleted macrophages using anti-CD8α and anti-CSFR1 antibodies respectively, prior to subcutaneous injection of *St3gal1*$^{-/-}$ TRAMP-C2 cells (**Figure 5J and Supplemental Figure 5C**). As observed previously, *St3gal1*$^{-/-}$ cells in IgG control mice failed to engraft (**Figure 5K**). Strikingly, depletion of $CD8^+$ T cells resulted in a 75% engraftment rate of *St3gal1*$^{-/-}$ cells suggesting that the failure to engraft was, at least in some part, due to tumour immune clearance (**Figure 5L**). Supporting the idea that

macrophages contribute to *St3gal1*-driven immune suppression in PC, analysis of tumour growth kinetics showed a delay in tumour growth in anti-CSFR1 treated mice (**Figure 5M**). Furthermore, targeting of macrophages also resulted in a 75% engraftment rate, demonstrating a key role for macrophages in mediating *St3gal1* driven immune suppression. Given that macrophages are not classically considered to have direct cytotoxic capabilities, we hypothesise that following depletion of St3gal1 and subsequently Siglec ligands, macrophages may be re-educated towards a pro-inflammatory phenotype which would have secondary effects on cytotoxic effector cells, driving anti-tumour immunity.

Discussion

A growing body of literature suggests that targeting glyco-immune checkpoints, specifically Siglec-7/9 may provide therapeutic benefit in several cancers, including Acute Lymphoblastic Leukaemia, pancreatic, breast and melanoma. However, although there have been multiple studies on glycosylation changes in PC, to date, there is no literature describing the expression of Siglec ligands in prostate tumours or the abundance of tumour associated-Siglec^{+} immune cells. Here, for the first time, we show that Siglec ligands are expressed in prostate glands and are elevated in patients exposed to hormone-based therapies. We also provide important data on the expression of Siglec-7 and Siglec-9 receptors within the prostate TIME. Critically, we demonstrate that transcript levels of these glyco-immune checkpoints are elevated in aggressive prostate tumours, and high levels of Siglec receptors are associated with a poor disease outcome. Using *in vivo* models, we have implicated the ST3Gal1-sialoglycan-Siglec axis in macrophage anti-tumour biology and provide proof-of-concept data suggesting that depleting ST3Gal1 associated sialoglycans or targeting their respective Siglecs may boost immune tumour clearance. These important findings provide the fundamental rationale to study glyco-immune checkpoints as a potential therapeutic strategy for the treatment of advanced PC.

Currently, patients who have advanced PC have no curative options available to them. ICB for the treatment of advanced PC offers some promise, however, to date complete responses to pembrolizumab ICB monotherapy have remained low. Recent reports have demonstrated that enzalutamide treatment has the capacity to reinvigorate the prostate TIME. Some studies suggest that AR targeting therapies may increase numbers of infiltrating immune cells in prostate tumours, although reports on this are conflicting (7,11). Recent studies trialling pembrolizumab in patients previously treated with enzalutamide (NCT02312557) have highlighted AR activity drives immunosuppression. Crucially, enzalutamide has been shown to act on the AR expressed in T cells to reduce T cell exhaustion, sensitising prostate tumours to ICB (63). However, this combination is effective in only a minority of patients. Immune

suppression for the majority is therefore maintained by AR independent mechanisms that are yet to be fully elucidated. Importantly, this demonstrates that prostate tumours have the necessary anti-tumour effectors required for an immunotherapy response, they just need to be unlocked.

Hyper-sialyation of solid tumours has previously been shown to be associated with an immunosuppressed TIME. Much of the work studying sialylation of prostate tumours has focused on α2'6-siaylation through the glycosyltransferases ST6Gal1 and ST6GalNAc1, which have been shown to be androgen regulated (22). In this current study we show that ST3Gal1 levels negatively correlate with AR signalling in PC however the mechanisms that underpin this remain unclear. Glycosyltransferases are known to be regulated by key oncogenic drivers including the AR. Previous reports on AR regulation of glycosylation have indicated that many of the enzymes involved in glycosylation are positively regulated by androgen signalling (25). AR can also act as a transcriptional repressor either through recruitment of co-factors or antagonism of other transcriptions factors such as MYC, which has been shown to directly drive ST3GAL1 transcription (64,65). Reactivation of MYC in response to AR targeting treatments has been identified as a driver of aggressive disease after first line therapy and may be one of the mechanisms which promote a reduction in ST3Gal1 levels when AR signalling is high, and an increase in ST3Gal1 in response to AR therapeutic targeting. Our study therefore demonstrates that AR control of glycosylation is multi-faceted and has therapeutic implications.

Like $CD8^+$ T cells, enzalutamide has been shown to directly affect AR activity in myeloid populations. This however drives an immunosuppressive switch, resulting in a pro-tumour macrophage phenotype (66). In this study, we provide insight into enzalutamide induced immune suppression by showing that enzalutamide treatment increases levels of ST3Gal1 and its associated immunosuppressive Siglec-7 and -9 ligands on the surface of PC cells. Previous studies have shown that Siglec-7 and Siglec-9 ligands are found on *O*-glycans (62,67–69). Siglec-7 and -9 and their murine equivalent Siglec-E have been shown previously to be important glyco-immune checkpoints, directly promoting a protumour macrophage phenotype which can suppress cytotoxic $CD8^+$ T cells (15,21,58). Taken together these data show that enzalutamide regulation of immune cell phenotype can be both direct, and indirect and can drive pro- and anti-tumour activity in a cell-type specific manner. We propose that this careful balance of pro- and anti-tumour activities can be tilted towards immune directed tumour clearance by therapies targeting the glyco-immune axis.

In summary, we report that ST3Gal1 synthesises Siglec-7 and Siglec-9 ligands which are critical to maintaining immune suppression in the prostate TIME and that targeting this axis may reactivate anti-tumour immunity. We demonstrate that this important glyco-immune checkpoint is upregulated by AR targeting therapies and may contribute to immune suppression and poor ICB response. Given the complexity of the glyco-immune axis, it will be important to interrogate the cell-type specific consequences of systemic therapies to better understand both the therapeutic and unintended effect of current standard of care treatments. Novel therapies targeting glyco-immune checkpoints are currently being developed and trialled, hence it is timely to determine how PC patients could benefit from these new therapies, and how they may be combined with current standard of care treatments.

Financial Support Statement

This work was funded by a Prostate Cancer UK Travelling Prize fellowship awarded to ES [TLD-PF19-002]. RG is supported by a William Edmond Harker Foundation Studentship. DG is funded by the Newcastle Cancer Research UK (CRUK) Clinical Academic Training Programme. ENS is supported by an Alberta Innovates Graduate fellowship. LW and CNR are supported by Cancer Research UK Experimental Cancer Medicine Centre funding [25160]. KH is supported by Prostate Cancer Research and The Mark Foundation for Cancer Research [6961]. DJE is supported by two Biotechnology and Biological Sciences Research Council grants [BB/S008039/1 and BB/W002019/1]. KC is supported by This work was supported by a Movember funded Prostate Cancer UK Career Development Fellowship [CDF12-006]. AH, AB and RH are supported by a Prostate Cancer Foundation Challenge Award [PCF (ref:18CHAL11)]. B.A. is supported by the Ken Bell Bursary and JGW Patterson Foundation [12/21 NU009331]. LW, RN and LG are supported by Prostate Cancer Research [PCR-6955]. MM is supported by NSERC and GlycoNet funding. JM is supported by Prostate Cancer UK through a Research Innovation Award and the Bob Willis Fund [RIA16-ST2-011].

Acknowledgements

We thank Michael Robson, Steve Smith and Melanie Williamson from the Newcastle University Comparative Biology Centre (CBC) for technical support with enzalutamide dosing of animals. We thank CBC staff for the animal husbandry, Newcastle University Bioimaging unit staff for support with fluorescent imaging, and Newcastle University Flow Cytometry Core Facility staff for assistance with flow cytometry.

Data Availability

All data presented in this study are available by request from the corresponding author.

References

1. Sung H, Ferlay J, Siegel RL, Laversanne M, Soerjomataram I, Jemal A, et al. Global Cancer Statistics 2020: GLOBOCAN Estimates of Incidence and Mortality Worldwide for 36 Cancers in 185 Countries. CA Cancer J Clin [Internet]. 2021 May 1 [cited 2022 Dec 20];71(3):209–49. Available from: https://onlinelibrary.wiley.com/doi/full/10.3322/caac.21660
2. Nuhn P, De Bono JS, Fizazi K, Freedland SJ, Grilli M, Kantoff PW, et al. Update on Systemic Prostate Cancer Therapies: Management of Metastatic Castration-resistant Prostate Cancer in the Era of Precision Oncology. Eur Urol. 2019 Jan 1;75(1):88–99.
3. Mateo J, Fizazi K, Gillessen S, Heidenreich A, Perez-Lopez R, Oyen WJG, et al. Managing Nonmetastatic Castration-resistant Prostate Cancer. Eur Urol. 2019 Feb 1;75(2):285–93.
4. Library WO, Rodrigues DN, Boysen G, Sumanasuriya S, Seed G, De Marzo AM, et al. The molecular underpinnings of prostate cancer: impacts on management and pathology practice. Wiley Online Library [Internet]. 2017 Jan 1 [cited 2022 Dec 20];241(2):173–82. Available from: https://onlinelibrary.wiley.com/doi/abs/10.1002/path.4826?casa_token=KC9ibMW8k-UAAAAA:3TQ-SOf72cKiAVqaXrk1TThnqFbeOXPRL4lNMc37NdY25c_NXopvAVeTKWl0P5hK7n4bTuaDDzHrK0o
5. Marcus L, Lemery SJ, Keegan P, Pazdur R. FDA Approval Summary: Pembrolizumab for the Treatment of Microsatellite Instability-High Solid Tumors. Clin Cancer Res [Internet]. 2019 [cited 2022 Dec 21];25(13):3753–8. Available from: https://pubmed.ncbi.nlm.nih.gov/30787022/
6. Antonarakis ES, Piulats JM, Gross-Goupil M, Goh J, Ojamaa K, Hoimes CJ, et al. Pembrolizumab for Treatment-Refractory Metastatic Castration-Resistant Prostate Cancer: Multicohort, Open-Label Phase II KEYNOTE-199 Study. J Clin Oncol [Internet]. 2020 Feb 10 [cited 2022 Dec 21];38(5):395–405. Available from: https://pubmed.ncbi.nlm.nih.gov/31774688/
7. Bansal D, Reimers MA, Knoche EM, Pachynski RK. Immunotherapy and Immunotherapy Combinations in Metastatic Castration-Resistant Prostate Cancer. Cancers 2021, Vol 13, Page 334 [Internet]. 2021 Jan 18 [cited 2022 Dec 21];13(2):334. Available from: https://www.mdpi.com/2072-6694/13/2/334/htm
8. Yu EY, Kolinsky MP, Berry WR, Retz M, Mourey L, Piulats JM, et al. Pembrolizumab Plus Docetaxel and Prednisone in Patients with Metastatic Castration-resistant Prostate Cancer: Long-term Results from the Phase 1b/2 KEYNOTE-365 Cohort B Study. Eur Urol [Internet]. 2022 Jul 1 [cited 2022 Dec 21];82(1):22–30. Available from: https://pubmed.ncbi.nlm.nih.gov/35397952/
9. Thoman ME, Salari K. Key Notes on Pembrolizumab and Docetaxel Combination Therapy for Metastatic Castration-Resistant Prostate Cancer. Eur Urol [Internet]. 2022 Jul 1 [cited 2022 Dec 21];82(1):31–3. Available from: https://pubmed.ncbi.nlm.nih.gov/35396162/
10. Yu EY, Piulats JM, Gravis G, Fong PCC, Todenhöfer T, Laguerre B, et al. Pembrolizumab plus Olaparib in Patients with Metastatic Castration-resistant Prostate Cancer: Long-term Results from the Phase 1b/2 KEYNOTE-365 Cohort A Study. Eur Urol [Internet]. 2023 Jan 1 [cited 2022 Dec 21];83(1). Available from: https://pubmed.ncbi.nlm.nih.gov/36055895/

11. Long X, Hou H, Wang X, Liu S, Diao T, Lai S, et al. Immune signature driven by ADT-induced immune microenvironment remodeling in prostate cancer is correlated with recurrence-free survival and immune infiltration. Cell Death Dis [Internet]. 2020 Sep 1 [cited 2022 Dec 19];11(9). Available from: /pmc/articles/PMC7502080/
12. Graff JN, Liang LW, Kim J, Stenzl A. KEYNOTE-641: a Phase III study of pembrolizumab plus enzalutamide for metastatic castration-resistant prostate cancer. Future Oncol [Internet]. 2021 Aug 1 [cited 2022 Dec 21];17(23):3017–26. Available from: https://pubmed.ncbi.nlm.nih.gov/34044584/
13. Graff JN, Beer TM, Alumkal JJ, Slottke RE, Redmond WL, Thomas G V., et al. A phase II single-arm study of pembrolizumab with enzalutamide in men with metastatic castration-resistant prostate cancer progressing on enzalutamide alone. J Immunother Cancer [Internet]. 2020 Jul 2 [cited 2022 Dec 21];8(2). Available from: https://pubmed.ncbi.nlm.nih.gov/32616555/
14. Läubli H, Pearce OMT, Schwarz F, Siddiqui SS, Deng L, Stanczak MA, et al. Engagement of myelomonocytic Siglecs by tumor-associated ligands modulates the innate immune response to cancer. Proc Natl Acad Sci U S A [Internet]. 2014 Sep 30 [cited 2022 Dec 21];111(39):14211–6. Available from: https://pubmed.ncbi.nlm.nih.gov/25225409/
15. Stanczak MA, Rodrigues Mantuano N, Kirchhammer N, Sanin DE, Jacob F, Coelho R, et al. Targeting cancer glycosylation repolarizes tumor-associated macrophages allowing effective immune checkpoint blockade. Sci Transl Med [Internet]. 2022 Nov 2 [cited 2022 Dec 21];14(669):eabj1270. Available from: https://www.science.org/doi/10.1126/scitranslmed.abj1270
16. Gray MA, Stanczak MA, Mantuano NR, Xiao H, Pijnenborg JFA, Malaker SA, et al. Targeted glycan degradation potentiates the anticancer immune response in vivo. Nature Chemical Biology 2020 16:12 [Internet]. 2020 Aug 17 [cited 2022 Dec 21];16(12):1376–84. Available from: https://www.nature.com/articles/s41589-020-0622-x
17. Barkal AA, Brewer RE, Markovic M, Kowarsky M, Barkal SA, Zaro BW, et al. CD24 signalling through macrophage Siglec-10 is a target for cancer immunotherapy. Nature. 2019;
18. Rodriguez E, Boelaars K, Brown K, Eveline Li RJ, Kruijssen L, Bruijns SCM, et al. Sialic acids in pancreatic cancer cells drive tumour-associated macrophage differentiation via the Siglec receptors Siglec-7 and Siglec-9. Nat Commun. 2021;12(1).
19. Scott E, Elliott DJ, Munkley J. Tumour associated glycans: A route to boost immunotherapy? Clinica Chimica Acta. 2020.
20. MacAuley MS, Crocker PR, Paulson JC. Siglec-mediated regulation of immune cell function in disease. Nature Reviews Immunology 2014 14:10 [Internet]. 2014 Sep 19 [cited 2022 Apr 29];14(10):653–66. Available from: https://www.nature.com/articles/nri3737
21. Ibarlucea-Benitez I, Weitzenfeld P, Smith P, Ravetch J V. Siglecs-7/9 function as inhibitory immune checkpoints in vivo and can be targeted to enhance therapeutic antitumor immunity. Proc Natl Acad Sci U S A [Internet]. 2021 Jun 29 [cited 2022 Dec 21];118(26):e2107424118. Available from: https://www.pnas.org/doi/abs/10.1073/pnas.2107424118
22. Munkley J, Scott E. Targeting Aberrant Sialylation to Treat Cancer. Medicines. 2019;
23. Garnham R, Scott E, Livermore KE, Munkley J. ST6GAL1: A key player in cancer. Oncology Letters. 2019.

24. Scott E;, Garnham R;, Cheung K;, Duxfield A;, Elliott DJ;, Scott E, et al. Pro-Survival Factor EDEM3 Confers Therapy Resistance in Prostate Cancer. International Journal of Molecular Sciences 2022, Vol 23, Page 8184 [Internet]. 2022 Jul 25 [cited 2022 Aug 5];23(15):8184. Available from: https://www.mdpi.com/1422-0067/23/15/8184/htm
25. Munkley J, Vodak D, Livermore KE, James K, Wilson BT, Knight B, et al. Glycosylation is an Androgen-Regulated Process Essential for Prostate Cancer Cell Viability. EBioMedicine. 2016;
26. Cerami E, Gao J, Dogrusoz U, Gross BE, Sumer SO, Aksoy BA, et al. The cBio Cancer Genomics Portal: An open platform for exploring multidimensional cancer genomics data. Cancer Discov. 2012;
27. Dunning MJ, Vowler SL, Lalonde E, Ross-Adams H, Boutros P, Mills IG, et al. Mining Human Prostate Cancer Datasets: The "camcAPP" Shiny App. EBioMedicine [Internet]. 2017 Mar 1 [cited 2023 Mar 14];17:5. Available from: /pmc/articles/PMC5360593/
28. Rodrigues E, Jung J, Park H, Loo C, Soukhtehzari S, Kitova EN, et al. A versatile soluble siglec scaffold for sensitive and quantitative detection of glycan ligands. Nat Commun. 2020;
29. Scott E, Hodgson K, Calle B, Turner H, Cheung K, Bermudez A, et al. Upregulation of GALNT7 in prostate cancer modifies O-glycosylation and promotes tumour growth. Oncogene [Internet]. 2023 Feb 1 [cited 2023 Mar 16]; Available from: https://pubmed.ncbi.nlm.nih.gov/36725887/
30. Tzeng SF, Tsai CH, Chao TK, Chou YC, Yang YC, Tsai MH, et al. O-Glycosylation–mediated signaling circuit drives metastatic castration-resistant prostate cancer. FASEB Journal. 2018 Dec 1;32(12):6869–82.
31. Hoadley KA, Yau C, Hinoue T, Wolf DM, Lazar AJ, Drill E, et al. Cell-of-Origin Patterns Dominate the Molecular Classification of 10,000 Tumors from 33 Types of Cancer. Cell [Internet]. 2018 Apr 5 [cited 2022 Dec 19];173(2):291-304.e6. Available from: http://www.cell.com/article/S0092867418303027/fulltext
32. Kounatidou E, Nakjang S, McCracken SRC, Dehm SM, Robson CN, Jones D, et al. A novel CRISPR-engineered prostate cancer cell line defines the AR-V transcriptome and identifies PARP inhibitor sensitivities. Nucleic Acids Res [Internet]. 2019 Jun 20 [cited 2022 Dec 19];47(11):5634–47. Available from: https://academic.oup.com/nar/article/47/11/5634/5475935
33. Antonarakis ES, Lu C, Wang H, Luber B, Nakazawa M, Roeser JC, et al. AR-V7 and resistance to enzalutamide and abiraterone in prostate cancer. N Engl J Med [Internet]. 2014 Sep 11 [cited 2022 Dec 19];371(11):1028–38. Available from: https://pubmed.ncbi.nlm.nih.gov/25184630/
34. Zhu Y, Dalrymple SL, Coleman I, Zheng SL, Xu J, Hooper JE, et al. Role of androgen receptor splice variant-7 (AR-V7) in prostate cancer resistance to 2nd-generation androgen receptor signaling inhibitors. Oncogene [Internet]. 2020 Nov 5 [cited 2022 Dec 19];39(45):6935–49. Available from: https://pubmed.ncbi.nlm.nih.gov/32989253/
35. Chen Z, Wu D, Thomas-Ahner JM, Lu C, Zhao P, Zhang Q, et al. Diverse AR-V7 cistromes in castration-resistant prostate cancer are governed by HoxB13. Proc Natl Acad Sci U S A. 2018 Jun 26;115(26):6810–5.
36. Sharp A, Coleman I, Yuan W, Sprenger C, Dolling D, Rodrigues DN, et al. Androgen receptor splice variant-7 expression emerges with castration resistance in prostate

cancer. J Clin Invest [Internet]. 2019 Jan 2 [cited 2022 Dec 19];129(1). Available from: https://pubmed.ncbi.nlm.nih.gov/30334814/

37. Nyquist MD, Corella A, Coleman I, De Sarkar N, Kaipainen A, Ha G, et al. Combined TP53 and RB1 Loss Promotes Prostate Cancer Resistance to a Spectrum of Therapeutics and Confers Vulnerability to Replication Stress. Cell Rep. 2020 May 26;31(8):107669.
38. Abida W, Cyrta J, Heller G, Prandi D, Armenia J, Coleman I, et al. Genomic correlates of clinical outcome in advanced prostate cancer. Proc Natl Acad Sci U S A [Internet]. 2019 [cited 2022 Dec 19];166(23):11428–36. Available from: https://pubmed.ncbi.nlm.nih.gov/31061129/
39. Grasso CS, Wu YM, Robinson DR, Cao X, Dhanasekaran SM, Khan AP, et al. The mutational landscape of lethal castration-resistant prostate cancer. Nature [Internet]. 2012 Jul 12 [cited 2022 Dec 19];487(7406):239–43. Available from: https://pubmed.ncbi.nlm.nih.gov/22722839/
40. Brockhausen I, Wandall HH, Hagen KG Ten, Stanley P. O-GalNAc Glycans. Essentials of Glycobiology [Internet]. 2022 [cited 2022 Dec 19]; Available from: https://www.ncbi.nlm.nih.gov/books/NBK579921/
41. Hugonnet M, Singh P, Haas Q, von Gunten S. The Distinct Roles of Sialyltransferases in Cancer Biology and Onco-Immunology. Front Immunol. 2021 Dec 17;12:5495.
42. Bojar D, Meche L, Meng G, Eng W, Smith DF, Cummings RD, et al. A Useful Guide to Lectin Binding: Machine-Learning Directed Annotation of 57 Unique Lectin Specificities. Cite This: ACS Chem Biol [Internet]. 2022 [cited 2022 Dec 19];2022:2993–3012. Available from: https://doi.org/10.1021/acschembio.1c00689
43. Xie Y, Sheng Y, Li Q, Ju S, Reyes J, Lebrilla CB. Determination of the glycoprotein specificity of lectins on cell membranes through oxidative proteomics. Chem Sci [Internet]. 2020 Sep 16 [cited 2022 Dec 19];11(35):9501–12. Available from: https://pubs.rsc.org/en/content/articlehtml/2020/sc/d0sc04199h
44. Cui HX, Wang H, Wang Y, Song J, Tian H, Xia C, et al. ST3Gal III modulates breast cancer cell adhesion and invasion by altering the expression of invasion-related molecules. Oncol Rep [Internet]. 2016 Dec 1 [cited 2023 Mar 14];36(6):3317–24. Available from: http://www.spandidos-publications.com/10.3892/or.2016.5180/abstract
45. Zhang N, Lin S, Cui W, Newman PJ. Overlapping and unique substrate specificities of ST3GAL1 and 2 during hematopoietic and megakaryocytic differentiation. 2022 [cited 2023 Mar 14]; Available from: http://ashpublications.org/bloodadvances/article-pdf/6/13/3945/1905504/advancesadv2022007001.pdf
46. Pietrobono S, Anichini G, Sala C, Manetti F, Almada LL, Pepe S, et al. ST3GAL1 is a target of the SOX2-GLI1 transcriptional complex and promotes melanoma metastasis through AXL. [cited 2023 Mar 14]; Available from: https://doi.org/10.1038/s41467-020-19575-2
47. Lin W Der, Fan TC, Hung JT, Yeo HL, Wang SH, Kuo CW, et al. Sialylation of CD55 by ST3GAL1 facilitates immune evasion in cancer. Cancer Immunol Res [Internet]. 2021 Jan 1 [cited 2023 Mar 14];9(1):113–22. Available from: https://aacrjournals.org/cancerimmunolres/article/9/1/113/470468/Sialylation-of-CD55-by-ST3GAL1-Facilitates-Immune

48. Stanczak MA, Siddiqui SS, Trefny MP, Thommen DS, Boligan KF, von Gunten S, et al. Self-associated molecular patterns mediate cancer immune evasion by engaging Siglecs on T cells. Journal of Clinical Investigation. 2018;128(11).
49. Wang J, Sun J, Liu LN, Flies DB, Nie X, Toki M, et al. Siglec-15 as an immune suppressor and potential target for normalization cancer immunotherapy. Nat Med. 2019;
50. Hudak JE, Canham SM, Bertozzi CR. Glycocalyx engineering reveals a Siglec-based mechanism for NK cell immunoevasion. Nat Chem Biol. 2014;
51. Jandus C, Boligan KF, Chijioke O, Liu H, Dahlhaus M, Démoulins T, et al. Interactions between Siglec-7/9 receptors and ligands influence NK cell-dependent tumor immunosurveillance. Journal of Clinical Investigation. 2014;
52. Beatson R, Tajadura-Ortega V, Achkova D, Picco G, Tsourouktsoglou TD, Klausing S, et al. The mucin MUC1 modulates the tumor immunological microenvironment through engagement of the lectin Siglec-9. Nat Immunol. 2016;
53. Ibarlucea-Benitez I, Weitzenfeld P, Smith P, Ravetch J V. Siglecs-7/9 function as inhibitory immune checkpoints in vivo and can be targeted to enhance therapeutic antitumor immunity. Proc Natl Acad Sci U S A [Internet]. 2021 Jun 29 [cited 2022 Dec 20];118(26). Available from: https://pubmed.ncbi.nlm.nih.gov/34155121/
54. Adeniji OS, Kuri-Cervantes L, Yu C, Xu Z, Ho M, Chew GM, et al. Siglec-9 defines and restrains a natural killer subpopulation highly cytotoxic to HIV-infected cells. PLoS Pathog [Internet]. 2021 Nov 1 [cited 2022 Dec 20];17(11). Available from: https://pubmed.ncbi.nlm.nih.gov/34762717/
55. Chen Z, Bai FF, Han L, Zhu J, Zheng T, Zhu Z, et al. Targeting Neutrophils in Severe Asthma via Siglec-9. Int Arch Allergy Immunol [Internet]. 2018 Feb 1 [cited 2022 Dec 20];175(1–2):5–15. Available from: https://pubmed.ncbi.nlm.nih.gov/29306942/
56. Jandus C, Boligan KF, Chijioke O, Liu H, Dahlhaus M, Démoulins T, et al. Interactions between Siglec-7/9 receptors and ligands influence NK cell-dependent tumor immunosurveillance. J Clin Invest [Internet]. 2014 Apr 1 [cited 2022 Dec 20];124(4):1810–20. Available from: https://pubmed.ncbi.nlm.nih.gov/24569453/
57. Beatson R, Tajadura-Ortega V, Achkova D, Picco G, Tsourouktsoglou TD, Klausing S, et al. The mucin MUC1 modulates the tumor immunological microenvironment through engagement of the lectin Siglec-9. Nat Immunol [Internet]. 2016 Oct 19 [cited 2022 Dec 20];17(11):1273–81. Available from: https://pubmed.ncbi.nlm.nih.gov/27595232/
58. Rodriguez E, Boelaars K, Brown K, Eveline Li RJ, Kruijssen L, Bruijns SCM, et al. Sialic acids in pancreatic cancer cells drive tumour-associated macrophage differentiation via the Siglec receptors Siglec-7 and Siglec-9. Nature Communications 2021 12:1 [Internet]. 2021 Feb 24 [cited 2022 Dec 20];12(1):1–14. Available from: https://www.nature.com/articles/s41467-021-21550-4
59. Erlandsson A, Carlsson J, Lundholm M, Fält A, Andersson SO, Andrén O, et al. M2 macrophages and regulatory T cells in lethal prostate cancer. Prostate [Internet]. 2019 Mar 1 [cited 2022 Dec 20];79(4):363–9. Available from: https://onlinelibrary.wiley.com/doi/full/10.1002/pros.23742
60. Siefert JC, Cioni B, Muraro MJ, Alshalalfa M, Vivie J, van der Poel HG, et al. The Prognostic Potential of Human Prostate Cancer-Associated Macrophage Subtypes as Revealed by Single-Cell Transcriptomics. Mol Cancer Res [Internet]. 2021 Oct 1 [cited 2022 Dec 20];19(10):1778–91. Available from: https://pubmed.ncbi.nlm.nih.gov/34131070/

61. Siddiqui S, Schwarz F, Springer S, Khedri Z, Yu H, Deng L, et al. Studies on the Detection, Expression, Glycosylation, Dimerization, and Ligand Binding Properties of Mouse Siglec-E. Journal of Biological Chemistry. 2017 Jan 20;292(3):1029–37.
62. Smith BAH, Deutzmann A, Correa KM, Delaveris CS, Dhanasekaran R, Dove CG, et al. MYC-driven synthesis of Siglec ligands is a glycoimmune checkpoint. Proceedings of the National Academy of Sciences [Internet]. 2023 Mar 14 [cited 2023 Mar 14];120(11). Available from: https://pnas.org/doi/10.1073/pnas.2215376120
63. Guan X, Polesso F, Wang C, Sehrawat A, Hawkins RM, Murray SE, et al. Androgen receptor activity in T cells limits checkpoint blockade efficacy. Nature 2022 606:7915 [Internet]. 2022 Mar 23 [cited 2023 Mar 14];606(7915):791–6. Available from: https://www.nature.com/articles/s41586-022-04522-6
64. Qiu X, Boufaied N, Hallal T, Feit A, de Polo A, Luoma AM, et al. MYC drives aggressive prostate cancer by disrupting transcriptional pause release at androgen receptor targets. Nature Communications 2022 13:1 [Internet]. 2022 May 13 [cited 2023 Mar 15];13(1):1–17. Available from: https://www.nature.com/articles/s41467-022-30257-z
65. Guo H, Wu Y, Nouri M, Spisak S, Russo JW, Sowalsky AG, et al. Androgen receptor and MYC equilibration centralizes on developmental super-enhancer. Nature Communications 2021 12:1 [Internet]. 2021 Dec 15 [cited 2023 Mar 15];12(1):1–18. Available from: https://www.nature.com/articles/s41467-021-27077-y
66. Consiglio CR, Udartseva O, Ramsey KD, Bush C, Gollnick SO. Enzalutamide, an androgen receptor antagonist, enhances myeloid cell-mediated immune suppression and tumor progression HHS Public Access. Cancer Immunol Res. 2020;8(9):1215–27.
67. Wisnovsky S, Möckl L, Malaker SA, Pedram K, Hess GT, Riley NM, et al. Genome-wide CRISPR screens reveal a specific ligand for the glycan-binding immune checkpoint receptor Siglec-7. Proc Natl Acad Sci U S A [Internet]. 2021 Feb 2 [cited 2023 Mar 30];118(5). Available from: https://pubmed.ncbi.nlm.nih.gov/33495350/
68. Büll C, Nason R, Sun L, Van Coillie J, Sørensen DM, Moons SJ, et al. Probing the binding specificities of human Siglecs by cell-based glycan arrays. Proc Natl Acad Sci U S A [Internet]. 2021 Apr 27 [cited 2023 Mar 30];118(17):e2026102118. Available from: https://www.pnas.org/doi/abs/10.1073/pnas.2026102118
69. Malaker SA, Pedram K, Ferracane MJ, Bensing BA, Krishnan V, Pett C, et al. The mucin-selective protease StcE enables molecular and functional analysis of human cancer-associated mucins. Proc Natl Acad Sci U S A [Internet]. 2019 Apr 9 [cited 2023 Mar 30];116(15):7278–87. Available from: https://www.pnas.org/doi/abs/10.1073/pnas.1813020116

Figure 1

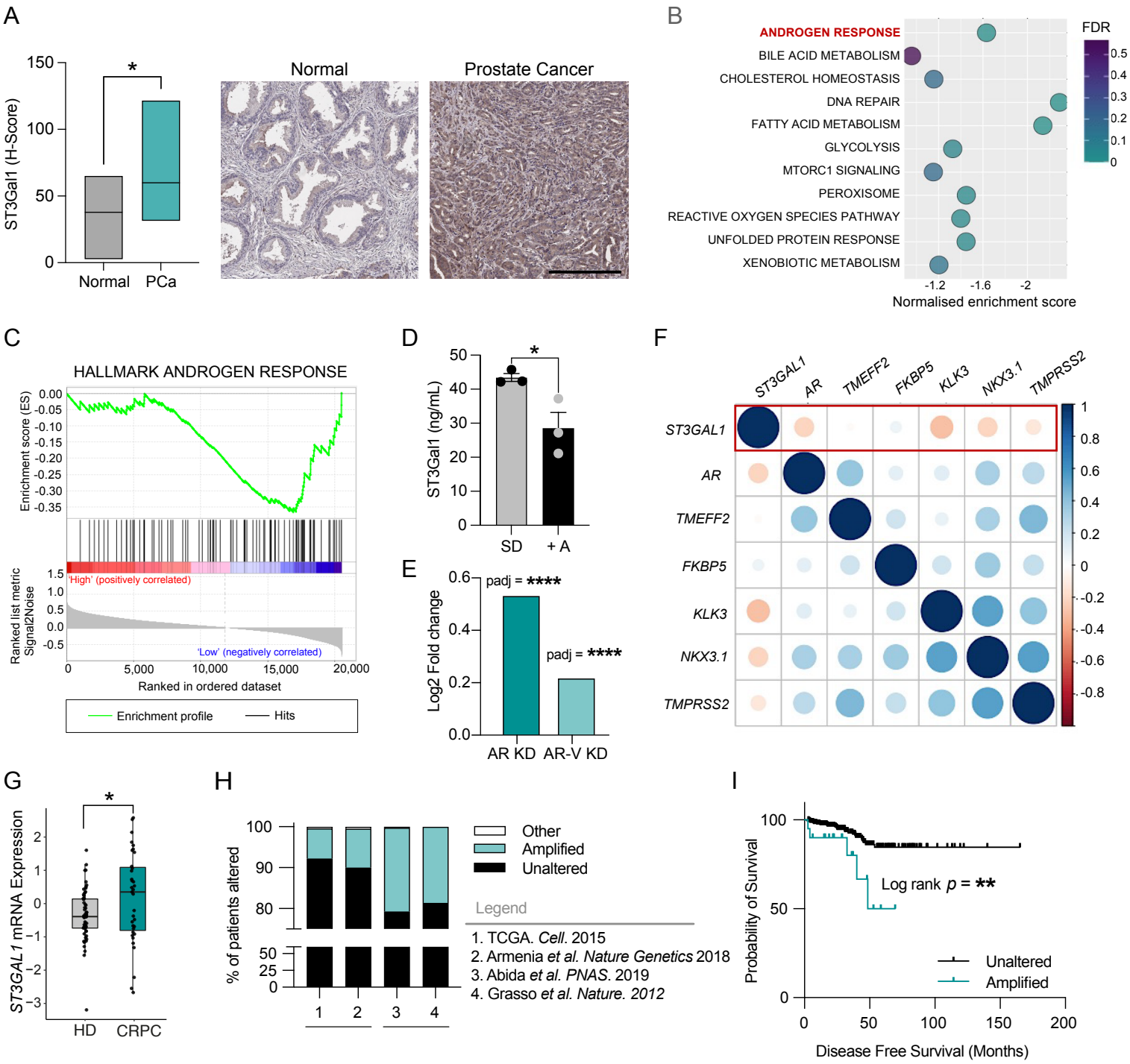

Figure 1. ST3Gal1 expression inversely correlates with androgen signaling in prostate cancer (A) Immunohistochemical detection of ST3Gal1 protein expression in normal prostate (N = 10) and prostate cancer (N=12) tissue samples. (B) Gene set enrichment analysis (GSEA) of The Cancer Genome Atlas (TCGA) Prostate Adenocarcinoma (PRAD) cohort. Patients were stratified based on *ST3GAL1* and the top and bottom quartiles compared (N = 250). Pathways negatively enriched in *ST3GAL1*^{high} patients are shown. FDR = False discovery rate. (C) GSEA for HALLMARK ANDROGEN RESPONSE in TCGA PRAD cohort. (D) Protein level quantification of ST3Gal1 expression in LNCaP cells cultured with or without 10 nm R1881 for 24 hours. (E) Quantification of *ST3GAL1* mRNA by RNA sequencing in CWR22Rv1 cells following siRNA knockdown of full-length AR or AR-variants. Statistics shown are adjusted p-value. (F) Correlation matrix correlogram showing *ST3GAL1* gene CRPC patients (N=138). Pearson's correlation coefficient is shown from −1 (red) to 1 (blue). Only correlations with statistical significance of $p < 0.05$ are shown. The size of the circle is proportional to the correlation coefficients. (G) Normalised *ST3GAL1* mRNA levels in publicly available RNA-sequencing in patients with CRPC compared to hormone dependent prostate cancer. (H) Meta-analysis of the percentage of patients with *ST3GAL1* genomic alternations across four independent prostate cancer patient cohorts. (TCGA N=498, Armenia *et al*. N=1013, Abida *et al*. N=444, Grasso *et al*. N=61). Cohort one and two are representative of hormone dependent (HD) cancers. Cohorts 3 and 4 represent CRPC patients. (I) Kaplan–Meier plot showing disease-free survival for prostate cancer patients based on unaltered and amplified *ST3GAL1* genomic alterations. Analysis includes N=498 patients from the TCGA PRAD cohort, accessed via CBioPortal. Significance tested using: Two-way t-test (A and D) and Long rank test (I). Statistical significance is shown as * $p < 0.05$, ** $p < 0.01$, *** $p < 0.001$ and **** $p < 0.0001$.

Figure 2

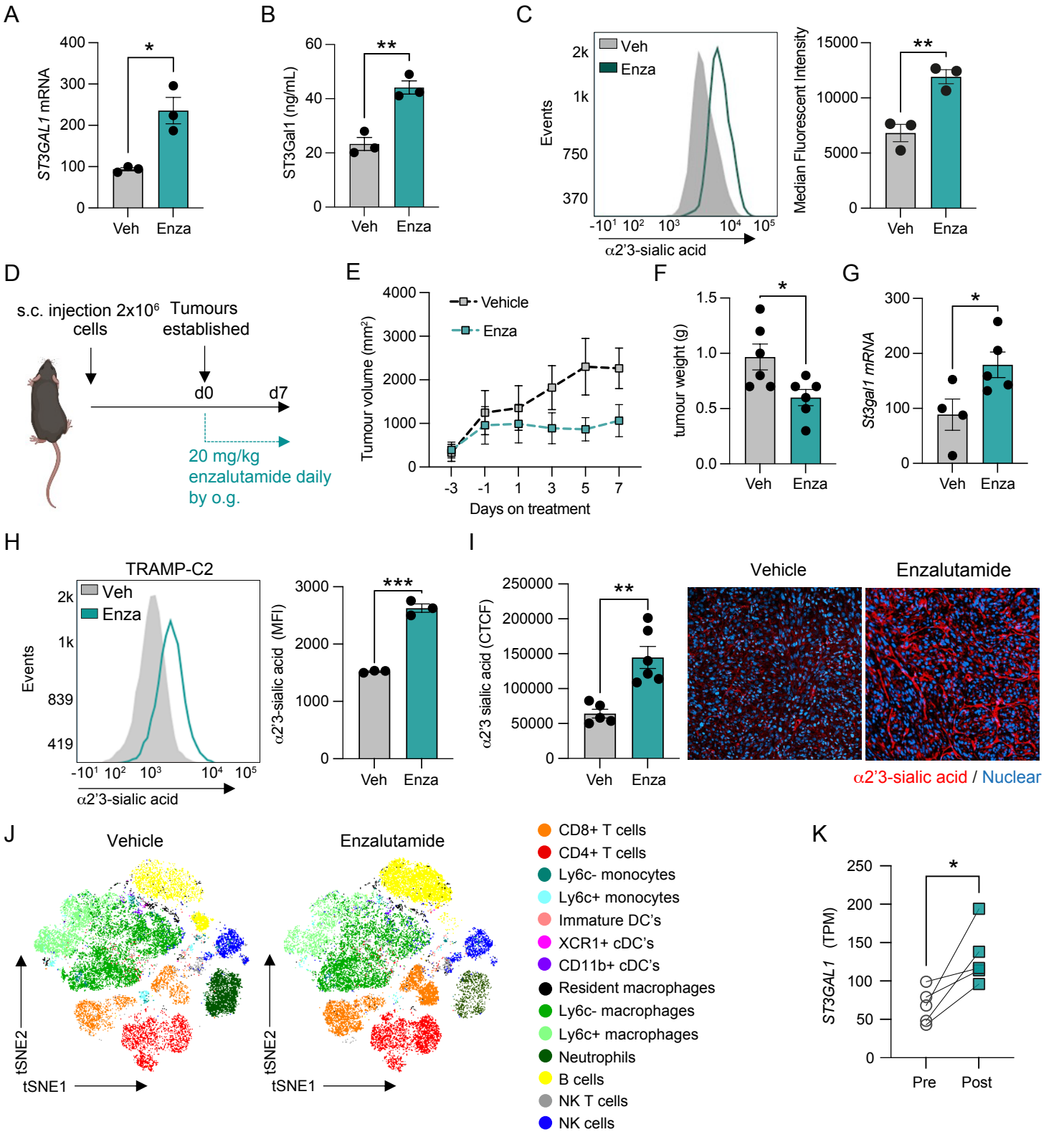

Figure 2. *Androgen receptor antagonism increases ST3Gal1 and α2-3-linked sialoglycans*

(A) *ST3GAL1* mRNA expression in LNCaP cells following 10 μM enzalutamide treatment measured by RT-qPCR (B) ST3Gal1 protein expression in LNCaP cells following 10 μM enzalutamide treatment quantified using a pre-validated ELISA. (C) MAL-II lectin detection of α2-3-sialylation in LNCaP cells following 10 μM enzalutamide treatment measured by flow cytometry. Representative histogram shown and bar chart of median fluorescent intensities. (D) Experimental design for TRAMP-C2 subcutaneous allografts in C57BL/6 mice treated with enzalutamide 20 mg/kg daily by oral gavage. (E) Tumour growth curves for subcutaneous allografts with 20 mg/kg enzalutamide treatment or vehicle control ($n = 6$ mice/group). (F) Tumour weights when tumours were harvested following 7 days enzalutamide treatment or vehicle control ($n = 6$ mice/group). (G) RT-qPCR analysis of *St3gal1* mRNA expression in TRAMP-C2 subcutaneous tumours following 7 days vehicle or enzalutamide treatment. (H) MAL-II lectin flow cytometry for cell surface α2-3-sialylation following 10 μM enzalutamide treatment for TRAMP-C2 cells. Representative histogram and bar chart with median fluorescent intensities shown. (I) MAL-II lectin immunofluorescence detection of α2-3-linked sialic acid (red) expression in FFPE subcutaneous TRAMP-C2 tumours treated with vehicle or enzalutamide. Data are corrected total cell fluorescence (CTFC). Representative images shown. (J) (t-distributed stochastic neighborhood embedding) tSNE maps of flow cytometric analysis of immune populations in subcutaneous allografts from vehicle and enzalutamide treated mice (K) ST3Gal1 gene expression levels determined by RNA sequencing of match biopsies pre and post enzalutamide treatment (n=5). Significance tested using two-way t-tests. Statistical significance is shown as * $p < 0.05$, ** $p < 0.01$, *** $p < 0.001$ and **** $p < 0.0001$.

Figure 3

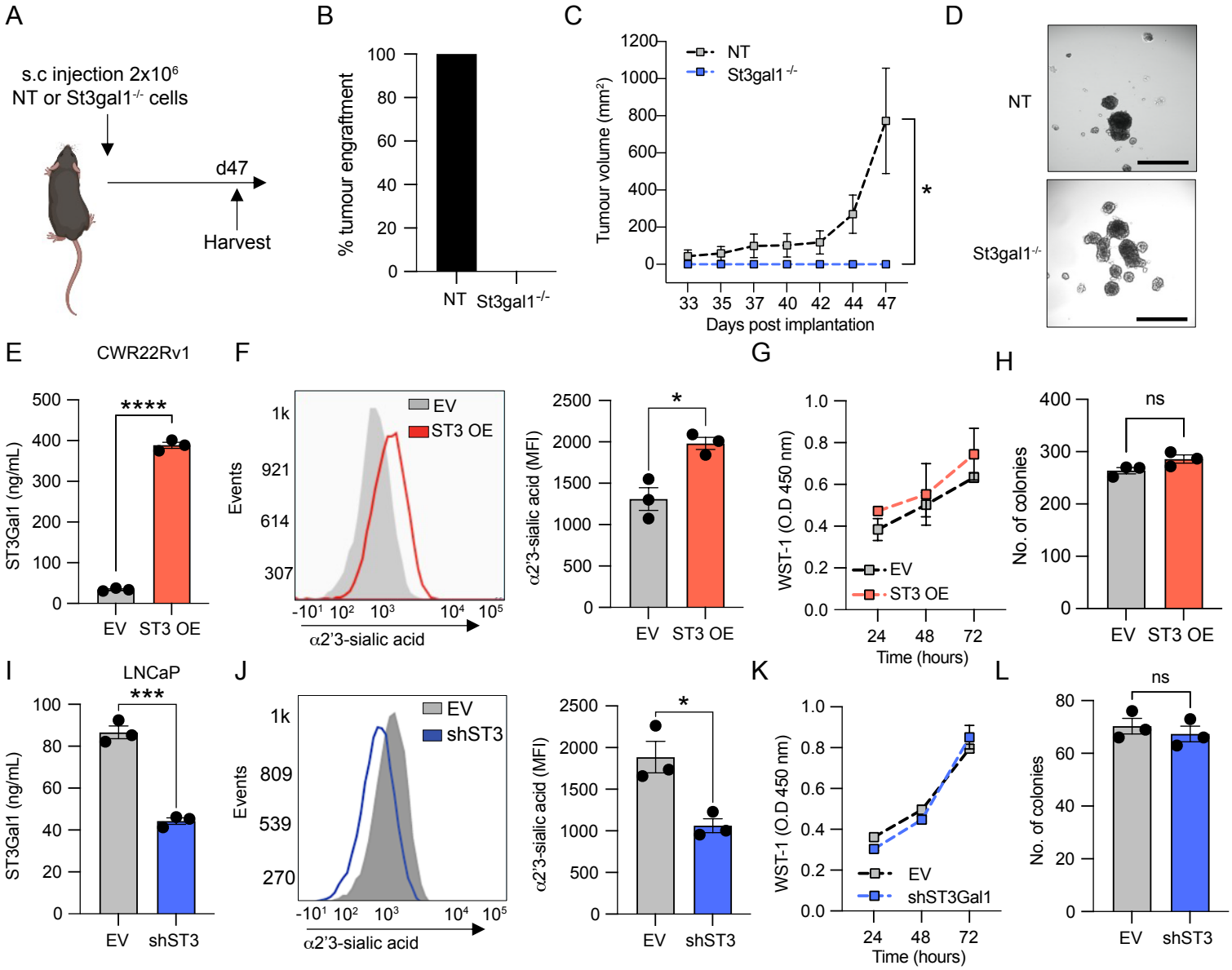

Figure 3. St3gal1-null cells fail to grow in C57BL/6 mice

(A) Schematic of *St3gal1*$^{-/-}$ TRAMP-C2 allograft experimental design. (B) Percentage tumour engraftment rate for non-targeting (NT) sgRNA control and *St3gal1*$^{-/-}$ TRAMP-C2 cells. N = 16 mice/group. (C) Tumour growth curves for NT and *St3gal1*$^{-/-}$ TRAMP-C2 allografts. (D) Representative images of NT and *St3gal1*$^{-/-}$ TRAMP-C2 spheroid formation *in vitro*. (E) Protein expression of ST3GAL1 in empty vector (EV) and *ST3GAL1* overexpression (OE) lentiviral transduced CWR22Rv1 cells. Levels quantified by ELISA. (F) Quantification of α2-3-sialylation in CWR22Rv1 EV and *ST3GAL1* OE cells using the MAL-II by flow cytometry. Representative histogram shown and bar chart of median fluorescent intensities. (G) Cellular proliferation of EV and *ST3GAL1* overexpression lentiviral transduced CWR22Rv1 cells quantified by WST-1 assay. Absorbance was read at 450 nm and normalised to background absorbance. (H) Colony forming ability of EV and *ST3GAL1* overexpression lentiviral transduced CWR22Rv1 cells measured using a colony forming assay. Graph shows number of colonies formed. (I) Protein expression of *ST3GAL1* in EV and shST3Gal1 knockdown lentiviral transduced LNCaP cells. Levels quantified by ELISA. (J) Quantification of α2-3-sialylation in LNCaP EV and sh*ST3GAL1* cells using the MAL-II by flow cytometry. Representative histogram shown and bar chart of median fluorescent intensities. (K) Cellular proliferation of EV and sh*ST3GAL1* lentiviral transduced LNCaP cells quantified by WST-1 assay. Absorbance was read at 450 nm and normalised to background absorbance. (L) Colony forming ability of EV and sh*ST3GAL1* lentiviral transduced LNCaP cells measured using a colony forming assay. Graph shows number of colonies formed. Significance tested using two-way t-tests. Statistical significance is shown as * $p < 0.05$, ** $p < 0.01$, *** $p < 0.001$ and **** $p < 0.0001$.

Figure 4

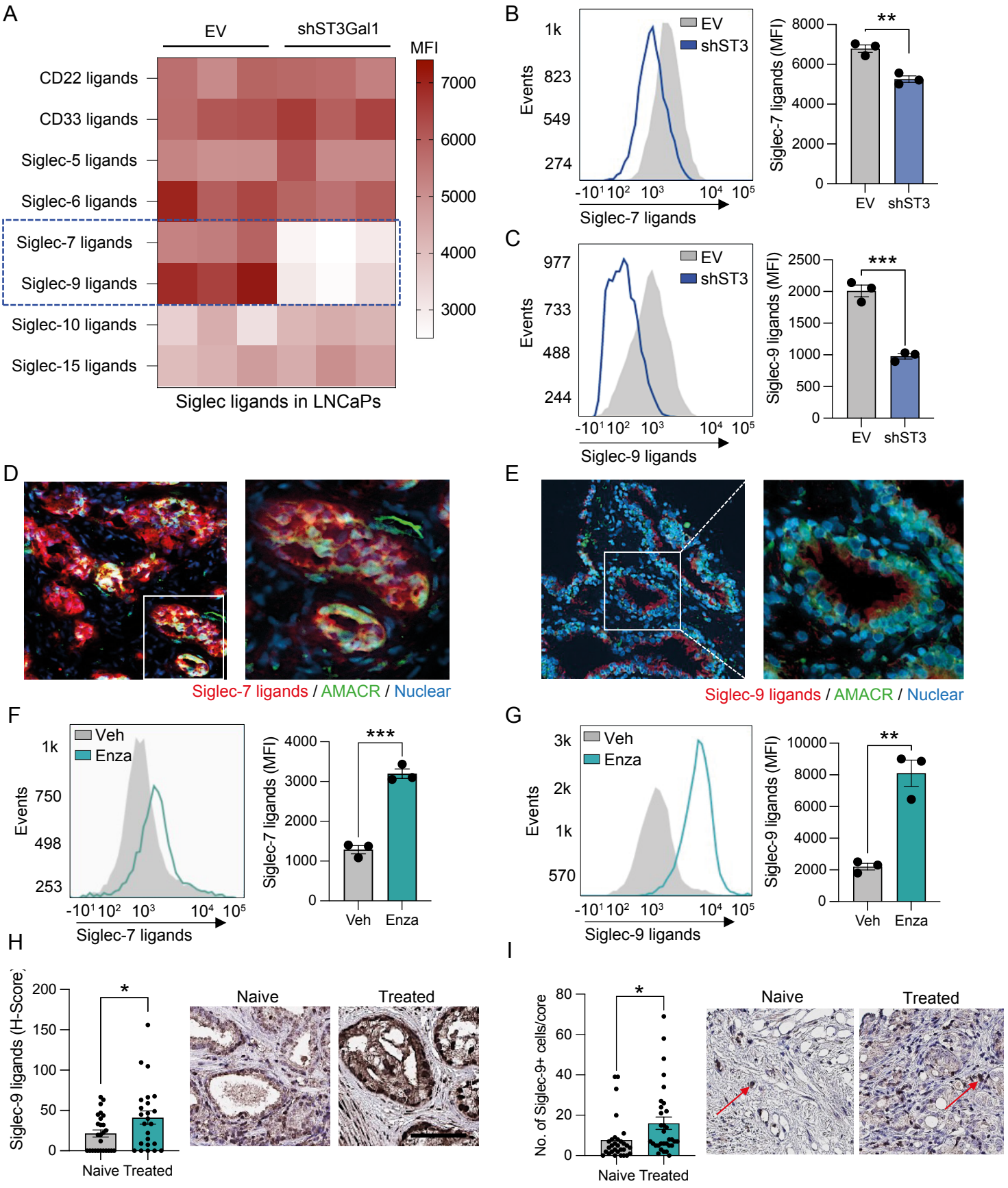

Figure 4. Siglec-7 and Siglec-9 ligands are synthesised by ST3Gal1 and upregulated by AR targeting therapies

(A) Heatmap showing siglec binding capabilities in LNCaP empty vector (EV) and sh*ST3GAL1* knockdown cells as determined by flow cytometry using Siglec-Fc reagents. Significant changes in Siglec-7 and Siglec-9 binding capacity are highlighted in the blue dashed box. Experiment was conducted in triplicate. Data are median fluorescent intensities. (B-C) Quantification of Siglec-7 and Siglec-9 binding capacity in CWR22Rv1 EV and sh*ST3GAL1* cells using Siglec-Fc reagents. Representative histogram and bar chart with median fluorescent intensities shown. (D) Siglec-7 ligands (red) colocalized with AMACR (green) in prostate cancer patient biopsies using dual immunofluorescence. Images prepared using a ZEISS Axio Imager2 microscope with a x20 and x40 objective. (E) Siglec-9 ligands (red) colocalized with AMACR (green) in prostate cancer patient biopsies using dual immunofluorescence. Images prepared using a ZEISS Axio Imager2 microscope with a x20 and x40 objective. (F) Quantification of Siglec-7 ligands using Siglec-Fc reagents in LNCaP cells treated with vehicle or 10 μM enzalutamide. Representative histogram and bar chart with median fluorescent intensities shown. (G) Quantification of Siglec-9 ligands using Siglec-Fc reagents in LNCaP cells treated with vehicle or 10 μM enzalutamide. Representative histogram and bar chart with median fluorescent intensities shown. (H) Immunohistochemistry detection of Siglec-9 ligands using Siglec-Fc reagents in a tissue microarray (TMA). Patients include those who are treatment naïve (N=26) and those who have been exposed to androgen deprivation therapy (N=24). H-scores were generated to quantify staining in epithelial cells using a Leica Aperio slide scanner. Representative images shown (I) Immunohistochemistry detection of Siglec-9 in a tissue microarray (TMA). Patients include those who are treatment naïve (N=30) and those who have been exposed to androgen deprivation therapy (N=32). The number of positive Siglec-9^{+} cells were quantified per tissue core. Representative images shown. Examples of Siglec-9^{+} ells highlighted with red arrows. Significance tested two-way t-tests. Statistical significance is shown as * $p < 0.05$, ** $p < 0.01$, *** $p < 0.001$ and **** $p < 0.0001$.

Figure 5

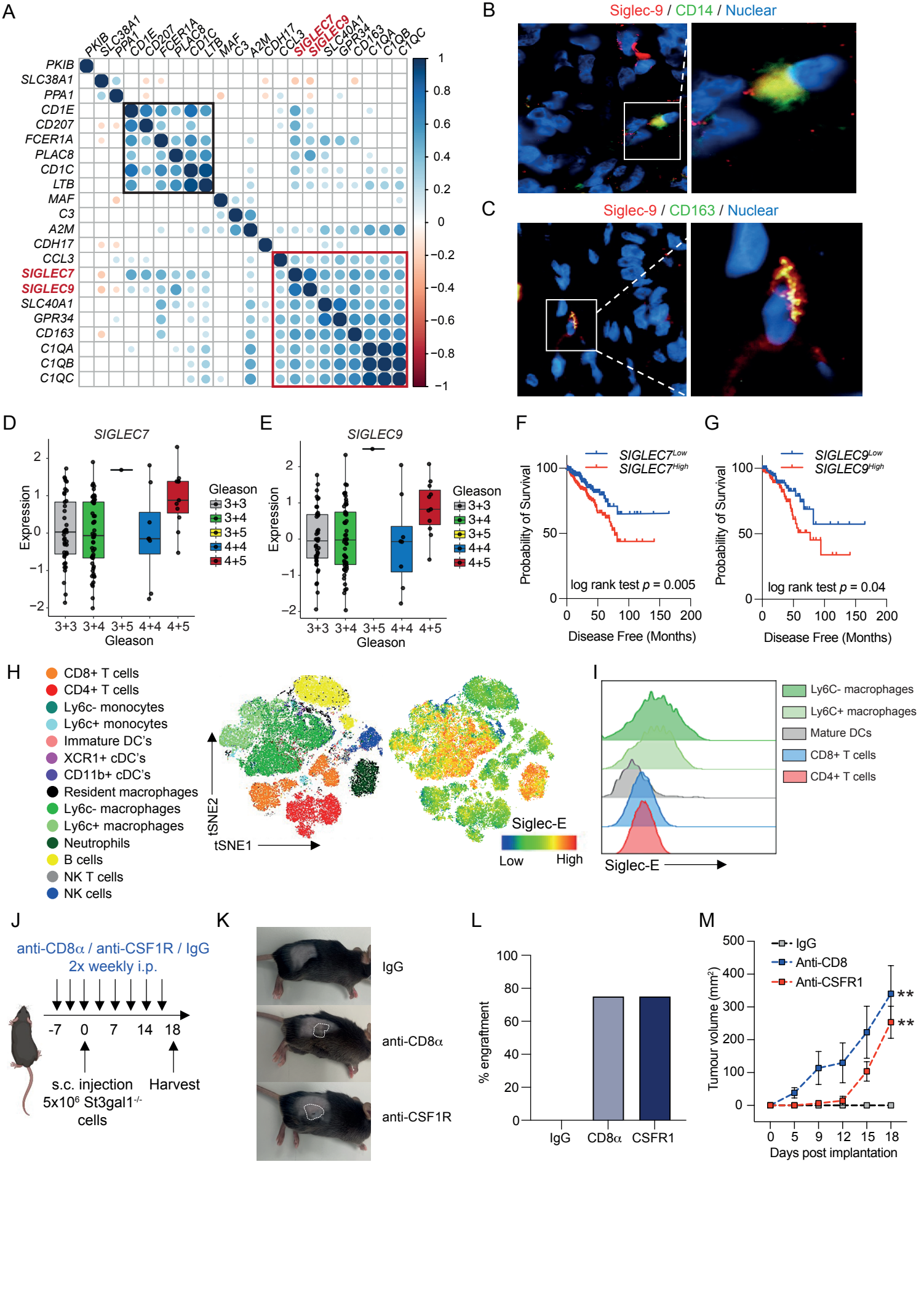

Figure 5. ST3Gal1 bio-synthesised siglec ligands are critical glyco-immune checkpoints in prostate cancer.

Correlation matrix correlogram correlating mRNA levels of *SIGLEC7* and *SIGLEC9* with a 19-gene prognostic macrophage signature in 208 CRPC patients in the SU2C dataset. Pearson's correlation coefficient is shown from −1 (red) to 1 (blue). Only correlations with statistical significance of $p < 0.05$ are shown. Circle size is proportional to the correlation coefficients. A pro-proliferative cluster is highlighted in the black box and anti-inflammatory cluster highlighted in the red box. (B-C) Dual immunofluorescence staining of Siglec-9 positive (red) myeloid cells with (B) the myeloid marker CD14 (green) and (C) alternatively activated macrophage marker CD163 (green) in prostate cancer patient biopsies. Images prepared using a ZEISS Axio Imager2 microscope with a X20 and X63 objective. (D-E) mRNA expression levels of *SIGLEC7* (D) and *SIGLEC9* (E) from RNA-sequencing of the MSKCC prostate cancer publicly available dataset. Data was accessed through camcAPP. (F-G) Kaplan–Meier plot showing disease-free survival for prostate cancer patients stratified based on low (bottom 50%) or high (top 50%) *SIGLEC7* (F) and *SIGLEC9* (G) gene expression. Analysis includes 498 prostate cancer patients from the TCGA PRAD cohort, accessed via CBioPortal. (H) t-distributed stochastic neighborhood embedding) tSNE maps of flow cytometric analysis of immune populations in TRAMP-C2 subcutaneous allografts. Siglec-E protein expression on immune cell subsets is shown. (I) Representative stacked histogram showing Siglec-E expression levels on immune subsets as determined by flow cytometry (J) Schematic of study design for T cell and macrophage depletion studies in *St3gal1*$^{-/-}$ subcutaneous allografts. (K) Representative photographs taken from mice at the end of the study. Tumours are highlighted with dashed white lines. (L) Bar chart showing percentage engraftment of *St3gal1*$^{-/-}$ TRAMP-C2 cells in mice following IgG, anti-CD8α or anti-CSFR1 treatment (M) Tumour growth curves for *St3gal*$^{-/-}$ TRAMP-C2 allografts in IgG control, anti-CD8α and anti-CSFR1 treated mice. Significance tested using: One-way ANOVA (D,E,L and M) and log rank (F and G). Statistical significance is shown as * $p < 0.05$, ** $p < 0.01$, *** $p < 0.001$ and **** $p < 0.0001$.